Improving the prediction capabilities of Binary Collision Approximation ion implant simulators

J.M. Hernández-Mangas, J. Arias, L. Bailón, M. Jaraíz, J. Barbolla
Dept. Electricidad y Electrónica, Universidad de Valladolid, Spain.
(September 26, 2001)

An efficient Binary Collision Approximation (BCA) ion implant code with good prediction capabilities in semiconductor materials (Si, GaAs SiC) with only one fitting parameter for low implantation doses is presented. It includes specific interatomic potentials and recent improvements in physical models for inelastic stopping. A periodic ab initio full bond electron density for the target is used. Damage accumulation is supported using a modified Kinchin-Pease model. Also some of the BCA integration algorithms and target selection procedure have been refined. An algorithm commonly used for statistical noise reduction has been modified to also improve the noise reduction in the lateral and shallow zones. The agreement with experiments is good, even under channelling conditions and for different target materials. A comparison with experimental SIMS results for several projectiles and targets is presented.

I. INTRODUCTION

Ion implantation is one of the main processes used for the fabrication of modern integrated microelectronic devices, allowing controlled doping of the active regions. The reliable prediction of dopant concentrations by simulations is of great importance in order to save the cost and time required by experiments.

Accurate knowledge of the three-dimensional profile of the implanted ions is crucial for current deep sub-micron devices, as this distribution is closely related to the desired electrical characteristics of the final device. The ability to accurately predict the lateral doping profiles as well as the depth profiles in a computationally efficient manner is important for optimum design and fabrication of advanced devices. Also dopant profiles implanted with high energies are needed to create retrograde wells. Channelling of projectiles into the target must be taken into account with physical models, because some projectiles (e.g. boron into silicon) present a strong channelling component [1–4].

To be predictive for different materials and projectiles, a simulation code must be able to simulate different implant conditions like angle, orientation, oxide layer, dose, etc., with the same set of adjustable parameters and models.

Also, the ion implant simulator must allow a trade-off between speed and accuracy [5]. All of these aspects have been studied by different groups and are now scattered across different simulation codes. In an effort to analyze the prediction capabilities and computational efficiency that can be attained with these models, we have gathered them all into a single simulation code. The purpose of this paper is, therefore, to first describe the models implemented and then present an analysis of the performance of the combined use of these models in terms of prediction capabilities and computational efficiency. We selected the binary collision approximation (BCA) in order to achieve this because, although the Molecular Dynamics (MD) technique is more accurate than BCA, it needs much longer calculation times. In addition, BCA methods can be refined to improve their accuracy to meet current needs.

Historically, researchers have used several modelization schemes to solve the problem of ion implantation. The choice depends on material's characteristics such as amorphous [6] or crystalline [7] targets, and also on the description level of the problem: MD, BCA, Transport Equation, etc.

In the 60's, the LSS theory [8,9] was introduced to model ion implantation. In this theory the total stopping power was calculated as the sum of two independent contributions: nuclear (elastic) and electronic (inelastic). The nuclear stopping was obtained by means of classical mechanics. The electronic stopping was assumed to be proportional to the ion velocity and it did not depend on either the ion direction or the individual collisions. This is a *non-local* stopping and sees the ion as moving in a uniform electron gas. This model did not follow the ion trajectory into the target and did not take into account the crystalline properties of the target.

An improved modelization was made in 1974 by Robinson et al. [7,10,11] (MARLOWE code). This model considers a crystalline target material with the BC approximation. It uses a symmetrically spherical electron density (ZBL density) that does not represent neither the bonds of covalent targets nor the low electron density at the interstitial zones. It also used integration algorithms that did not take into account the effect of the neighboring atoms potential energy. As a result, it had a low predictive capability, it needs a number of fitting parameters to match the experiments. This code has been greatly modified by many authors (e.g. [1,12])

A third simulation scheme for ion implantation was developed by Ziegler, Biersack and Littmark (ZBL) [6] in 1985. It was a BCA Monte Carlo method for amorphous targets. The projectile trajectory is statistically followed selecting randomly a target atom, an impact parame-

ter and a distance (mean free path). The elastic part of the collision was solved by classical mechanics obtaining the new position, direction and energy for both the projectile and target atom. To shorten the calculation time it uses a *magic formula* that fits the solved equations. The inelastic contribution was estimated using the Brandt and Kitagawa theory [13]. It had two terms: the proton stopping in a uniform electron gas, and a scaling factor for heavier projectiles. The proton stopping was fitted through experimental data.

This model works sensibly well for amorphous targets, but it cannot be employed for crystalline targets.

A highly modified MARLOWE code (UT-MARLOWE) was developed [1,14–16] at the University of Texas at Austin. It covered the most commonly used implant species into single crystal silicon with explicit dependence on energy, dose, tilt and rotation angles, but the models used for stopping, damage, etc., are different depending on species, energy range, etc. in order to match the experimental results.

CRYSTAL-TRIM [2] code was a combination between the MARLOWE and TRIM codes in order to be fast with amorphous targets, but it uses many adjustable parameters [17] both for the electronic stopping and the damage model to cover all the implant species and conditions.

The University of Wien has developed VISTA-MCIMPL that also needs many fitting parameters to match experiments. It implements a complex rare-event model [18].

Other attempts to model ion implantation have been made using mixtures of the ones cited above or using MD. Molecular Dynamics is very time consuming (orders of magnitude more than BCA). However, in the near future, MD may be the technique of choice for very low energies.

Our starting point has been the MARLOWE scheme [7] but it has been completely rewritten in C++ [12,19,20]. A physical model with only one adjustable parameter [21] has been used for the electronic stopping using a novel integration method. Also to speed-up the simulator a new statistical noise reduction scheme has been implemented.

II. PHYSICAL MODELS

Projectiles are simulated following their complete trajectory as well as the trajectories of the recoils generated (full cascade development). The target material is modelled as crystalline, polycrystalline or amorphous [7]. For polycrystalline targets a random rotation of the whole crystal is made before each ion implant. For amorphous, a random rotation of the crystal is done before each collision.

Thermal vibrations are considered using a Debye temperature model. The RMS amplitude of the thermal displacement varies with the target temperature as $A_{RMS} = 12.063464\,(A(T)/(T_{Debye}M))^{1/2}$ where M is the atomic mass, T_{Debye} is the Debye temperature of the target obtained experimentally [22] and $A(T)$ is the Debye function [23].

Projectiles loose their energy both elastically and inelastically by collisions with the atoms of the target material. The binary collision approximation, used here, considers only the collision with one target atom at a time. Simultaneous collisions are modelled through a combination of individual collisions [10] when needed (e.g. channeling conditions).

The scheme followed iteratively is: (i) search of target candidates (as in Ref. [7]); (ii) calculation of each binary (individual) elastic collision; (iii) selection of actual targets; (iv) calculation of *non-local* electronic losses for each binary collision considering the 3D periodic electron density following the asymptotic trajectories (tabulating this procedure with the actual trajectories would lead to a too high computational burden); (v) calculation of *local* electronic losses for the simultaneous collision with all the targets; (vi) finally, energy and momentum conservation rules are applied and projectile and targets are moved to their new positions. Specific explanations of these steps will be given next.

A. Elastic losses: specific screening functions

The nuclear interaction between the incident projectile and the target atom is solved by classical mechanics [24]. A numerical integration of the movement equations for both particles is done. To speed up the implant simulation, a look-up table is previously calculated. A repulsive Coulombic screened potential is used. The screening function can be selected among several universal and specific ones. By default a universal screening function due to ZBL [6] is used.

Other universal screening functions (Bohr, Molière [25], Lenz-Jensen [26], Thomas-Fermi [27]) have been tested [28]. We use specific screening functions, when available, for each projectile-target combination obtained by ab-initio methods [6] (e.g. with DMol code [29]) to reduce the number of approximations used by the simulator. When no specific screening function is available the best suited seems to be the ZBL one. It has a mean error of 2.1% with respect to specific ones [6].

B. Inelastic losses: physical models

It has been found necessary [21] to include inelastic energy loss due to collisions (*local*), and energy loss due to background electronic stopping (*non-local*) as two distinct mechanisms in order to obtain good simulation results under a range of channelling conditions [28,30,31]. It is not possible to assume that one of these processes is dominant and fit it to accurately model energy losses for different implant energies and directions.

The *non-local* inelastic stopping accounts for the average energy loss of the ion as it travels along the interstitial volume of the target. It is due to the interaction between the nucleus of the projectile and the target's electrons. This electronic stopping is given by the modified Brandt-Kitagawa [13] theory with only one adjustable parameter [4,32], r_s^0. This stopping is calculated as

$$S_{non\_local} = \int_{trajectory} [Z_1^*(v, r_s^0)]^2 S_p(v, r_s) dx \qquad (1)$$

where Z_1^* represents the effective charge of the ion, S_p is the electronic stopping power for a proton and $r_s = (3/(4\pi\rho))^{1/3}$ the one-electron radius (ρ is the local electron density). The r_s^0 value is related to the effective electron density of the target and depends on the ion-target combination [4].

According to Brandt and Kittagawa the effective charge is defined as: $Z_1^* = Z_1\gamma(v, r_s^0)$ with

$$\gamma(v, r_s^0) = q(v) + C(r_s^0)(1 - q(v)) \ln\left[1 + \left(\frac{4\Lambda}{r_s^0}\right)^2\right] \qquad (2)$$

where $q(v)$ is the ionization fraction, $C(r_s^0)$ depends weakly on the target, but can be approximated to 0.5 and

$$\Lambda = \frac{2a_0(1 - q(v))^{2/3}}{Z_1^{1/3}\left[1 - (1 - q(v))/7\right]} \qquad (3)$$

where $a_0 = 0.24005$. The ionization fraction, $q(v)$ is dependent on the relative velocity between the ion and the target. A scaling variable, defined as $y_r = v/(v_B Z_1^{2/3})$ where v_B is the Bohr velocity, is used to match an experimentally measured ($3 \leq Z_1 \leq 92$) curve for the ionization fraction [6,33] following a velocity criterium for stripping electrons $q = 1 - \exp(0.803y_r^{0.3} - 1.3167y_r^{0.6} - 0.38157y_r - 0.008983y_r^2)$.

We have tested [28] other formulae for the ionization fraction with a velocity criterium [13] or with an energy criterium [34], but the best results have been obtained with the formula cited above.

The proton stopping depends on the local electron density that results from the crystalline structure of the target. For low energies, a numerical approximation to the model of Echenique et al. [35] is used. For high energies Bethe's model [36] is used.

For the electron density we use a three-dimensional electron charge distribution for crystalline silicon, that includes the covalent tetrahedrical bonds, calculated by the ab initio pseudo-potential total energy method in the local density approximation [37]. For other target materials the electron density can be obtained in the same way.

The *local* inelastic energy loss stopping is related with the close collisions and take into account the electron-electron interaction between the projectile and target atoms. It is described by the modified Firsov theory [38,39] as proposed by Beardmore et al. [21]: $\Delta E_i = \int_{trajectory} F_{ij} dr$ where

$$F_{ij} = \frac{2^{1/3}\hbar}{2\pi a_B}(\hat{v}_j - \hat{v}_i) \left[Z_A^2 I\left(\frac{Z_A^{1/3}\alpha R}{a}\right) + Z_B^2 I\left(\frac{Z_B^{1/3}(1-\alpha)R}{a}\right)\right] \qquad (4)$$

with

$$I(W) = \int_W^\infty \frac{\Phi^2(x)}{x} dx \qquad (5)$$

and $\alpha = \left[1 + (Z_B/Z_A)^{1/6}\right]^{-1}$, $\Phi(x)$ being the universal screening function [6], Z_A, Z_B the atomic numbers ($Z_A \geq Z_B$), R the atomic separation, $a = (9\pi^2/128)^{1/3} a_B$, and a_B the Bohr radius. As mentioned by Firsov [39], at sufficiently high ion velocities the electrons of the two atoms will not have the time necessary for free interaction, and therefore the transfer of energy will diminish. Following Ref. [40] we have accounted for this fact by damping out the energy transfer beyond a critical velocity ($v_c = 0.7 v_B$, where v_B is the Bohr velocity), as:

$$\Delta E_i^* = \Delta E_i \begin{cases} v/v_B & \text{for } v < v_c \\ v_c^2/(v v_B) & \text{for } v \geq v_c \end{cases} \qquad (6)$$

In order to obtain a smooth transition between the lower and upper velocity regions, a transfer function [41] is used:

$$f(v) = \frac{2\exp\left(-(v/v_c)^2\right)}{1 + \exp\left(-2(v/v_c)^2\right)} \qquad (7)$$

Finally,
$S_{local} = f(v)\Delta E^*_{i,low\ vel} + (1 - f(v))\Delta E^*_{i,high\ vel}$.

C. Three-dimensional electron density distribution

The local electron density distribution is also used for the calculation of the *non-local* inelastic stopping. It is very important to match ends by periodicity to reduce the computation inaccuracies. The ZBL electron density is a spherically symmetric electron distribution calculated by Ziegler et al. [6] and was used by several authors [4,17,42]. It has a uniform interstitial density that does not represent the density of the open channels accurately (Figure 1). The 3D electron density used by us is obtained by means of the ab initio pseudo-potential total energy method in the local density approximation [37]. This provides a full description of the covalent bonds of the target material. We have also used a 3D electron density that we call Isolated Atom Density Superposition (IADS). This approximation is closer to the true bond

density than the ZBL one. We expected this should be a good approximation for non-polar covalent materials (e.g. silicon).

Figure 1 shows the differences between the ZBL, IADS and true bond densities along the {111} direction for a silicon target. It is clear that the ZBL density does not represent accurately some regions (in particular, interstitial regions).

A comparison between the common electron distributions [28,30,31], reveals the necessity for a three-dimensional description of the covalent nature of silicon. This necessity is extensible, and even more important, for other compound semiconductors. For silicon targets the main differences were observed in the {110} channel direction [28]. Simulations without free parameters [43] have also proven the necessity of using a 3D electron density distribution.

D. Damage accumulation

In order to deal with high dose implantations the simulator must include some damage accumulation model. It will be important especially in channelling cases. Although we have implemented the full cascade development, due to practical reasons (mainly the speed of the simulator) we have begun implementing damage accumulation based on Kinchin-Pease theory [1,44] as a first approximation. In a near future we plan to include the full cascade development in damage accumulation as a slower but more accurate option. The modelization of damage has two parts: the *defect generation/recombination* and the *damage simulation*. The damage simulation will be described in the Computing Algorithms section.

The number of point defects generated, n, is proportional to the energy, E, lost by nuclear scattering in each sector:

$$n = \frac{kE}{2E_d} \tag{8}$$

where $k = 0.8$ is a constant and E_d is the displacement threshold energy. For boron implantation into silicon $E_d = 15$ eV. Part of the point defects generated recombines with other defects, so the net increase of point defects after recombination, Δn, is given by:

$$\Delta n = n f_{surv}(1 - \frac{N}{N_\alpha}) \tag{9}$$

where f_{surv} is the fraction of point defects surviving both intracascade and intercascade recombination and it is adjusted for each implanted kind of projectile (e.g. $f_{surv} = 0.06$ for boron into silicon), N is the previous local defect density, and N_α is the local defect density necessary to reach amorphization (e.g. for silicon N_α is ten percent of the atomic density).

III. COMPUTING ALGORITHMS

A. Inelastic losses: integration methods

We have observed that the integration schemes for the two energy loss components can play a critical role in order to achieve the degree of accuracy demanded by current technology, particularly under channeling conditions. As a result, we are using an integration method that is a hybrid between molecular dynamics and the BCA model, in order to improve the numerical integrations.

For the *non-local* electronic losses the straight projectile incoming trajectory is sampled (see Fig. 2, where a straight movement is considered for the projectile between P_1 and P_2 and target from T_1 to T_2) having into account the potential energy at each point due to the surrounding neighbors, $E_p(x)$, the elastic energy transfer to the target, $E_T(x)$, and also the electronic losses accumulated upto this point, $S_{non\_local}(x)$. The local kinetic energy for the projectile is calculated as: $E_c(x) = E_{c0} - E_T(x) - S_{non\_local}(x) - E_p(x)$ where E_{c0} is the initial kinetic energy at this collision. The $E_T(x)$ value is calculated by linear interpolation between its initial and final values. Since $v = \sqrt{2E_c/M_1}$ the *non-local* electronic losses can be integrated using equation (1).

The *local* inelastic losses are integrated along the straight incoming and outgoing trajectories (Figure 2) of the projectile. Straight displacements are assumed for the target. At each point, the force F_{ij} between the projectile and the target is evaluated using equation (4). The outgoing trajectory is followed long enough to account for all the interaction. At this stage we consider the contributions of the electron densities of all the targets involved in the collision.

B. Statistical noise improvement algorithm

In order to reduce the calculation time and to improve the accuracy of the simulated profiles a three-dimensional rare event algorithm is implemented [45]. The straightforward way to obtain a statistically significant concentration at all depths of the profile is to run many simulated cascades. Most of the ions will stop near the main peak. The majority of the computer effort will not improve the accuracy of the tail or low concentration zones. With the atom splitting scheme [45] at certain depths, the ion is split into two *virtual* ions with half statistical weight of unsplit ion. The *virtual* ions generated have the same position and velocity as the parent ion. Their final trajectories are, however, different due to the thermal vibration effects. In the end, we obtain practically the same number of *virtual* ions at each bin of the histogram profile improving the statistics on low concentration zones. In the ion implant simulation there are two rare event cases of particular interest to be considered to

improve the statistics of the impurity profile: the deep region (channeled ions) and the shallow region.

1. Channelled ions

This case occurs when the projectile travels through a crystal channel. It looses its energy mainly by inelastic interaction without experiencing hard nuclear (elastic) collisions. We monitor the total distance travelled by the ion to improve statistics at both the deep and the lateral regions.

In general, we define a border d_i as either a depth reached by the ion or as the total distance travelled by the projectile. When the ion reaches the border with the next index, it is splitted into two *virtual* ions with half statistical weight. Figure 3 shows an example of how a real ion is split several times into several *virtual* ions when it reaches certain borders. We also show the statistical weight associated with each *virtual* ion. The borders cited above are calculated by solving the following equation

$$\int_0^{d_i} C(x)dx = (1-(1/2)^i)\int_0^{\infty} C(x)dx \qquad (10)$$

where $C(x)$ is the dopant histogram profile at a certain depth (or total distance travelled) x.

With this scheme we can recalculate the splitting borders dynamically in order to improve the statistics in specific regions. We do not need to know *a priori* the borders. First, N_0 real ions are simulated without the rare event algorithm, in order to obtain some statistics to estimate the initial borders d_i. Then, the algorithm is activated and the borders are recalculated every $N_{interval}$ real ions. This value must be large enough (e.g. $N_{interval} = 100$) so that the computation time is not increased noticeably. When we have attained the desired statistical accuracy in the rare event region, the algorithm is automatically deactivated.

Figure 4 shows the dopant profiles obtained for an implantation of boron into silicon with 2 keV, with and without the trajectory-length selection scheme. We observe the better definition of the profile tail. The simulation time is doubled with the algorithm, but the time needed to obtain the same accuracy without the algorithm would have been 10 times longer [45].

2. Projectiles in the shallow region of the impurity profile

When we simulate medium and high energy implants there is some statistical noise in the shallow region of the profiles due to the (few) ions that have lost their energy at the beginning of their trajectory. We use two conditions to identify these projectiles:

First, an energetic condition: the energy decreases below a user defined threshold energy, $E \leq E_{th}$, that is generally a percentage of the initial energy. Ions that verify this condition are likely to stop nearby.

Second, a positional condition: we consider the shallow region (Fig. 5) defined by $W_{shallow} = p_d(D_{max} - D_{min})$, where D_{max} is the maximum depth reached by an implanted ion, D_{min} is the positive minimum depth of the current profile and p_d is the percentage of the whole profile that the user considers to be the shallow region. We divide $W_{shallow}$ into N equal zones. Initially the projectile is considered to have index 0 ($n_{index} = 0$, with unity statistical weight). When the first condition ($E \leq E_{th}$) is met we compare the current depth of the projectile, $D_{projectile}$ with the border that defines the next index as $D_{projectile} < D_{min} + W_{shallow}(1 - n_{index}/N)$.

If the two conditions are met we split the current ion into two virtual half-weighted ions and we increment n_{index}. And the same procedure is applied to both virtual ions again. Finally, the algorithm is deactivated when the statistical accuracy required is reached.

Figure 6 shows a retrograde implant profile of boron into silicon with and without the shallow region enhancement scheme. We note the better definition of that region. The simulation time is increased by 50% with respect to not using the algorithm, but the time necessary to obtain the same statistical accuracy by increasing the number of projectiles simulated (by ten), increases the time by a 7.6 factor in this case [45].

C. Damage accumulation

As defined above our damage model is based on the modified Kinchin-Pease model [1,44] and its modelization has two parts: the *defect generation/recombination* and the *damage simulation*. Surface recess by sputtering is not accounted for in this simulator but this effect is negligible in the examples shown.

For the defect generation/recombination, in 1D, the crystal is divided into slices perpendicular to the depth axis. Equations 8 and 9 are applied to each sector to calculate its defect density. In order to reduce the computational overload generated by following the complete cascade a simplification can be used [15,44]. The simulator considers only the primary ion. When a scattering event occurs the energy transferred to the target atom E_T is compared with a cut-off energy (e.g. $E_{CutOff} = 24$ eV, for boron into silicon). If E_T is greater than the cut-off energy then the algorithm considers only a transferred energy of $E_T = E_{CutOff}$. This energy is defined as the energy needed to amorphize completely a sector as the result of a single collision. This approximation does not take into account the energy deposited by secondary atoms. The calculation time reduction using this approximation is about 30 %. The N_α and f_{surv} parameters depend on E_{CutOff} value.

In the damage simulation, for a given dose Φ, we define the area of the sectors as $A = N_{ions}/\Phi$, where N_{ions} is

the total number of real ions to be simulated. We apply periodic boundary conditions at the lateral borders of each sector. The local defect density, N, is a measure of the amorphization of each sector in the crystal. If the sector is completely amorphous, a random rotation of the crystal lattice is performed for each collision as in MARLOWE [7]. For a partially amorphized section the rotation probability is N/N_α. After the collision, the original crystal orientation is restored.

D. Speeding up the calculation

Several strategies have been employed throughout the code to speed up the calculation. When possible, lookup tables [12] previously calculated are used: elastic interaction, *local* and *non-local* inelastic losses, etc. The tables are calculated and stored in disk, for future use, for each projectile-target atom combination.

E. Selection of the target atoms

BCA needs a method to select the next target atoms to collide with. We begun using the MARLOWE [7] target atom selection method. It accepts target atoms that are in the direction of ion movement and have an impact parameter smaller than a given value ($p < p_{max}$) and a front distance $\xi > \xi_{min}$, where ξ_{min} was obtained from the last collision [11] to prevent successive collisions with the same target atom. After verifying the identical behavior between MARLOWE and our simulator for selecting the target atoms, step by step. We observed that, randomly, the selection mechanism missed a target atom or re-collided with the same atom. This is due to the thermal vibrations, that displaces the target atom from its lattice position. To avoid this wrong behavior, that mainly modifies the channelling tail, we store a list with the atoms involved in the last collision. We compare the new targets with the old ones, and remove the repeated ones. This replaces the ξ_{min} condition.

IV. RESULTS

In this section we compare simulated dopant profiles with experimental ones or with results from other simulators in order to asses our implementation of the ion implant BCA simulation and to test its prediction capabilities.

A. Silicon target

We first compare our simulation results with results from the well-known and validated TRIM amorphous simulator [6]. Since the profile shape is the same, Figure 7 shows only the projected range versus projectile energy for boron, arsenic and phosphorous implants into amorphous silicon. A very good agreement is obtained. Simultaneous collision treatment is necessary to correctly simulate [10] the channelling effect in crystalline targets. Since TRIM was designed for amorphous materials, it does not include such treatment. However, at low velocities, there are simultaneous collisions even in amorphous materials. This leads to an underestimation of the stopping by TRIM that is more relevant at low velocities (heavy ions, low energies), as can be seen in the inset of Fig. 7 for As.

For crystalline targets we compare our simulation results directly with SIMS experimental profiles obtained from the literature [16,21,32,42]. Figures 8, 9 and 10 represent boron implanted into silicon for several energies and implant conditions showing good agreement with experiments including very low energy (Fig. 8), channelling conditions (Fig. 9) and high energy (Fig. 10). All implants use the same (and only) fitting parameter $r_s^0 = 1.85$.

Figures 11, 12 and 13 show implants of arsenic into silicon for several energies and implant conditions. For this ion-target combination we use $r_s^0 = 2.0$ for all conditions.

In Figure 14 we can see phosphorous into silicon implants also with several energies and implant conditions. The value employed for r_s^0 is 1.85, identical to the boron-silicon case.

Figure 15 shows a high dose, $8 \cdot 10^{15}$ at/cm^2, boron into silicon implants for 15 and 80 keV and presents a good agreement with SIMS profiles.

These examples show the prediction capabilities of the models implemented in our simulator for a wide range of implant conditions (orientation, energy, etc.). To be able to simulate a new ion species only one fitting parameter, r_s^0 would have to be optimized.

B. Silicon carbide target

In order to further check the prediction capabilities of our modelization, we show some implant examples into 6H-SiC with several projectiles. Ion implantation is almost the only current method to dope silicon carbide. We used the IADS electron density approach and so we only fitted the r_s^0 parameter.

Figure 16 shows an aluminum implant into 6H-SiC. The tilt angle is 12.5° and the rotation is 30°. The orientation of the wafer flat is $\{11\bar{2}0\}$ and the wafers are cut 3.5° off-axis from the $\{0001\}$ plane toward the $\{11\bar{2}0\}$ direction. We compare the simulation results of 30, 90, 195, 500 and 1000 keV aluminum implants with the SIMS experimental [46] profile. A very good agreement is found. For Al into SiC we use $r_s^0 = 1.70$, which is not too different from the values used for the silicon target implants. We use the same damage accumulation parameters as for

silicon.

Figure 17 represents 40, 100 and 300 keV arsenic implants into 6H-SiC with the same conditions cited above ($r_s^0 = 1.75$). Again, they match very well.

C. Other target materials

Other interesting semiconductor materials are the III-V semiconductors, like gallium arsenide. Special characteristics for this material are a very low Debye temperature (360 K) and its softness. The damage accumulation will be important even for low doses ($N_\alpha = 6 \cdot 10^{20}$ at/cm^3, $f_{surv} = 0.09$).

Figure 18 shows silicon into GaAs (REO: Random Equivalent Orientation) and {100} channel, $r_s^0 = 2.0$) implants at 150 keV, $3 \cdot 10^{13}$ at/cm^2 compared with SIMS profiles [47], and it shows a comparison between selenium into GaAs (REO and {100} channel, $r_s^0 = 1.7$) implants at 300 keV, $3 \cdot 10^{13}$ at/cm^2, and SIMS profiles [47].

V. CONCLUSIONS

A new BCA ion implant simulator is reported. It gathers some of the best physical models and simulation algorithms, including a novel hybrid integration scheme for the inelastic energy losses. It also uses an *ab initio* physical description of the electron distribution for the target atoms. For low implant doses, the simulator is capable of predicting the impurity implant profiles for a wide range of projectile atoms and target materials with only one adjustable parameter (r_s^0) for each projectile-target material combination. For high doses, there are two additional fitting parameters (f_{surv}, N_α).

ACKNOWLEDGMENTS

This work was performed under the auspices of the Junta de Castilla y León (VA 14/00B) and the DGICYT project No. PB 98-0398.

VI. REFERENCES

[1] Kevin M. Klein, Changae Park, and A.F. Tasch. *IEEE Trans. Elect. Dev.*, 39(7):1614–1621, 1992.

[2] M. Posselt. *Rad. Eff. Def. Sol.*, 130, 1994.

[3] Cheruvu S. Murthy and G.R. Srinivasan. *IEEE Trans. Elect. Dev.*, 39(2):264–273, 1992.

[4] David Cai, Niels Gronbech-Jensen, C.M. Snell, and K.M. Beardmore. *Phys. Rev. B*, 54(23):17147–17157, 1996.

[5] International Technology Roadmap for Semiconductors. *Semiconductor Industry Association*, 1999.

[6] J.F. Ziegler, J.P. Biersack, and U. Littmark. Pergamon Press, New York, 1985.

[7] Mark T. Robinson and Ian M. Torrens. *Phys. Rev. B*, 9(12):5008–5024, 1974.

[8] J. Lindhard and M. Scharff. *Phys. Rev.*, 124:128–130, 1961.

[9] J. Lindhard, M. Scharff, and H.E. Schiott. *Dan. Vidensk. Seksk. Mat. Fys. Medd.*, 33(14):1–42, 1963.

[10] Mark Hou and Mark T. Robinson. *Nucl. Instr. and Meth.*, 132:641–645, 1976.

[11] Mark T. Robinson. *Phys. Rev. B*, 40(16):10717–10726, 1989.

[12] J. Arias, M. Jaraiz, L. Pelaz, L. Bailón, and J. Barbolla. *Nucl. Instr. and Meth. B*, 102:228–231, 1995.

[13] W. Brandt and M. Kitagawa. *Phys. Rev. B*, 25(9):5631–5637, 1982.

[14] S.H. Yang, S. Morris, S. Tian, K. Karab, A.F. Tasch, P.M. Echenique, R. Capaz, and J. Joannopoulos. In *Mat. Res. Soc. Symp.*, 1995.

[15] G. Wang, S. Tian, M. Morris, B. Obradovich, G. Balamurugan, and A. Tasch. *Microelectronic Device Technology, Austin TX, USA, SPIE-Int., Soc. Opt. Eng.*, pages 324–333, 1997.

[16] University of Texas at Austin. http://homer.mer.utexas.edu/TCAD/utmarlowe, 1999.

[17] Matthias Posselt, Bruno Schmidt, Thomas Feudel, and Norbert Strecker. *Materials Science Engineering B*, 71:128–136, 2000.

[18] W. Bohmayr, A. Burenkov, J. Lorenz, H. Ryssel, and S. Selberherr. *IEEE Trans. Semic. Manuf*, 8(4):402–407, 1995.

[19] J. Arias, M. Jaraiz, J.E. Rubio, L. Pelaz, L.A. Marqués, and J. Barbolla. *Journal Mat. Sci. and Tech.*, 11:1191–1193, 1995.

[20] J. Arias, J. Hernández, M. Jaraiz, L. Bailón, and J. Barbolla. In *Conferencia de Dispositivos Electrónicos*, Barcelona, 1997.

[21] Keith M. Beardmore and Niels Gronbech-Jensen. *Phys. Rev. E*, 57(6):7278–7287, 1998.

[22] G. Buschhorn, E. Diedrich, W. Kufner, M. Rzepka, H. Genz, P. Hoffmann-Stascheck, and A. Richter. *Phys. Rev. B*, 55(10):6196–6202, 1997.

[23] Charles Kittel. *Introducción a la física del estado sólido.* Reverté, Barcelona, 1993.

[24] J.B. Marion. *Classical dynamics of particles and systems.* Academic Press, Inc., New York, 1986.

[25] G. Moliere. *Z.f. Naturforsch*, A2:133, 1947.

[26] W. Lenz. *Z.f. Physik*, 77:713, 1947.

[27] A. Sommerfeld. *Z.f. Physik*, 77:722, 1932.

[28] Jesús Hernández. PhD thesis, University of Valladolid, Valladolid, Spain, 2000.

[29] DMol is a trademark of Bio Sym Inc., San Diego, CA., 2000.

[30] J. Hernández, M. Jaraiz, J. Arias, L. Bailón, J. Barbolla, A. Rubio, and J.L. Orantes. In *Conferencia de Dispositivos Electrónicos*, Madrid, 1999.

[31] J. Hernández, M. Jaraiz, J. Arias, J. Barbolla, L. Bailón, and A. Rubio. In *Mat. Res. Soc. Spring Meeting*, San Francisco, 1998.
[32] David Cai, C.M. Snell, Keith M. Beardmore, and N. Gronbech-Jensen. *Int. J. Modern Physics C*, 9(3):459–470, 1998.
[33] S. Kreussler, C. Varelas, and W. Brandt. *Phys. Rev. B*, 23(82), 1981.
[34] Richard J. Mathar and Matthias Posselt. *Phys. Rev. B*, 51(1):107–116, 1995.
[35] P.M. Echenique, R.M. Nieminen, and R.H. Ritchie. *Solid State Communications*, 37:779–781, 1981.
[36] H.A. Bethe. *Ann. Phys. (N.Y.)*, 5:325, 1930.
[37] Angel Rubio. (private communication). Dpto. Física Teórica, Facultad de Ciencias, Univ. de Valladolid, 1997.
[38] L.M. Kishinevskii. *Bull. Acad. Sci. USSR, Phys Ser*, 26:11433, 1962.
[39] O.B. Firsov. *Sov. Phys. JETP*, 36:1076–1080, 1959.
[40] S. Morris, D. Lin, S.H. Yang, S. Tian, K. Parab, and A.F. Tasch. In *Mat. Res. Soc. Symp. Proc.*, Vol. 396:27, 1996.
[41] M.J. Dort, P.H. Woerlee, and A.J. Walker. *Solid State Electronics*, 37(3):411–414, 1994.
[42] K.M. Klein, C. Park, and A.F. Tasch. *Nucl. Instr. and Meth. B*, 59/60:60–64, 1991.
[43] J. Sillampää, K. Nordlund, and J. Keinonen. *Phys. Rev. B*, 62(5):3109–3116, 2000.
[44] G.H. Kinchin and R.S. Pease. *Rep. Progress Phys.*, 18:1–51, 1955.
[45] J.M. Hernández-Mangas, J.Arias, M. Jaraíz, L. Bailón, and J. Barbolla. *Nucl. Instr. and Meth. B*, 174:433–438, 2001.
[46] S. Ahmed, C.J. Barbero, T.W. Sigmon, and J.W. Erickson. *J. Appl. Phys.*, 77(12):6194–6200, 1995.
[47] R.G. Wilson and V.R. Deline. *Appl. Phys. Lett.*, 37(9):793–796, 1980.
[48] P. Packman, H. Kennel, S. Thompson, S. Corcoran, and M. Taylor. In *11th Int. Conf, on Ion Implantation Technology*, pages 539–542, 1997.

VII. FIGURES

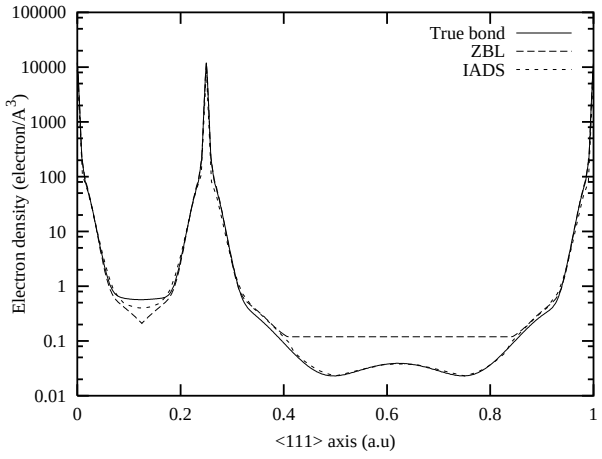

FIG. 1. Differences between ZBL, IADS and true bond densities along {111} direction.

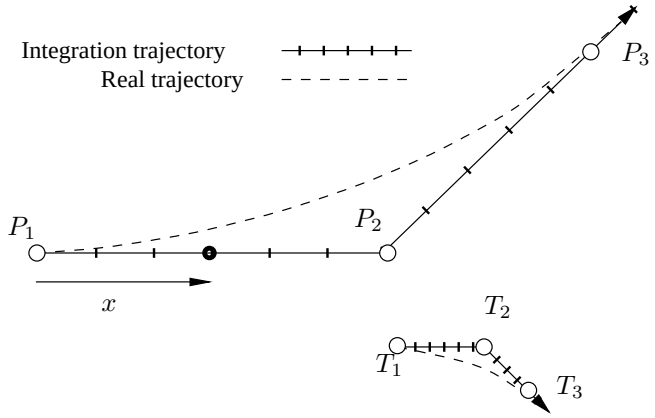

FIG. 2. Schematics for the *local* and *non-local* inelastic stopping integration algorithms.

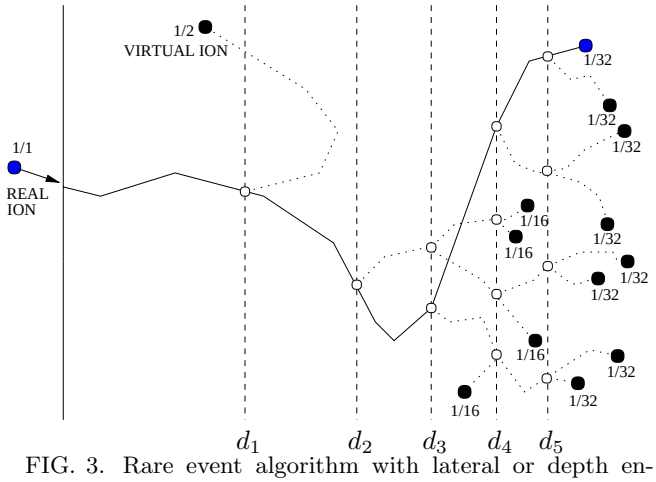

FIG. 3. Rare event algorithm with lateral or depth enhancement scheme.

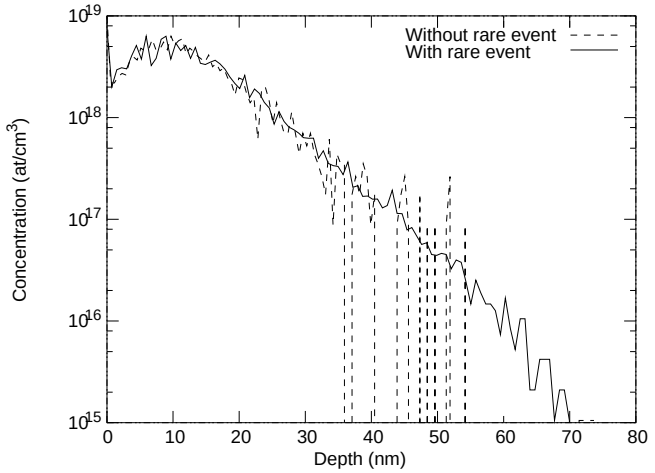

FIG. 4. Implantation of B (tilt=7°, rotation=30°) → Si {100}, 2 keV simulated with $N_{ion} = 2000$ real ion with and without the trajectory-length selection scheme.

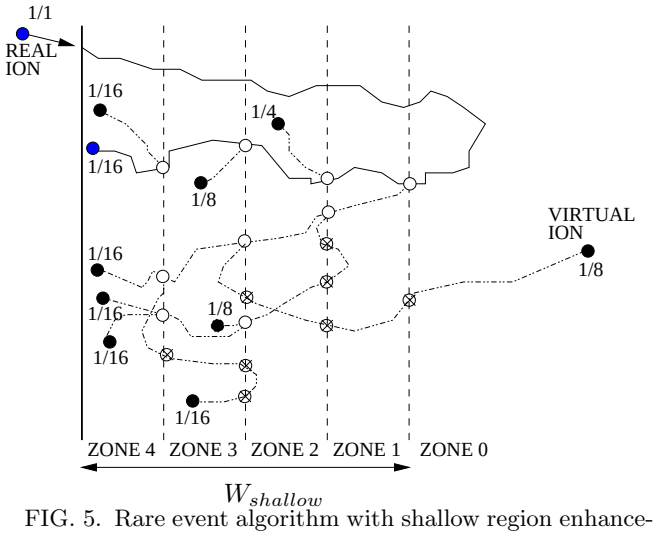

FIG. 5. Rare event algorithm with shallow region enhancement scheme.

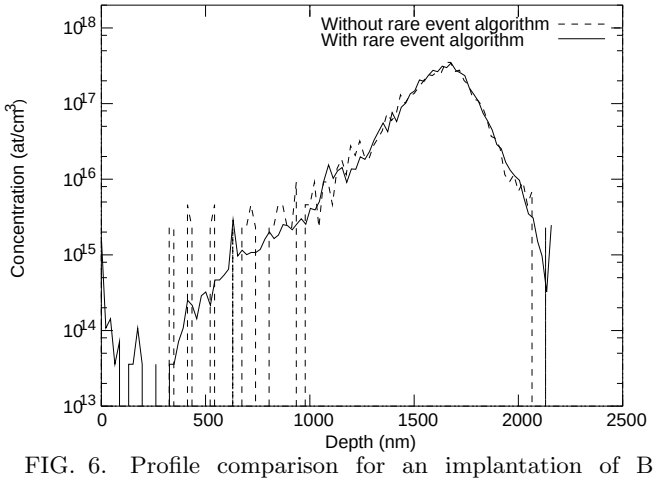

FIG. 6. Profile comparison for an implantation of B (7°,30°) → Si {100}, 1 MeV simulated with $N_{ion} = 2000$ real ion with an without the shallow region enhancement scheme.

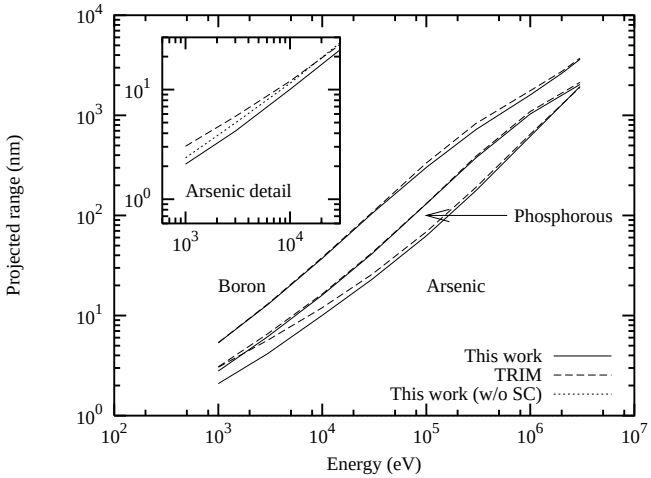

FIG. 7. Boron, Phosphorous and Arsenic into amorphous silicon. Comparison between TRIM and this work simulation results. The inset shows, for arsenic, the differences found with and without the simultaneous collision (SC) treatment.

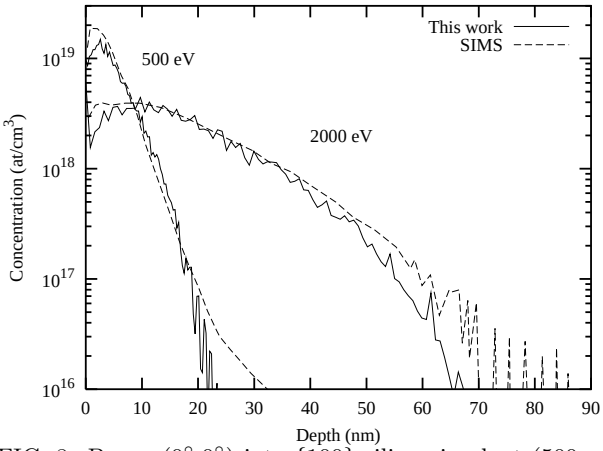

FIG. 8. Boron (0°,0°) into {100} silicon implant (500 and 2000 eV) comparison between SIMS profiles [21] and the current work simulation results.

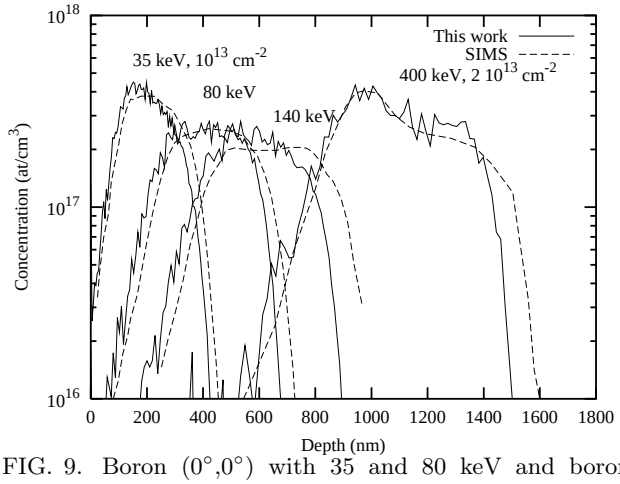

FIG. 9. Boron (0°,0°) with 35 and 80 keV and boron (0.6°,0°) with 140 and 400 keV implants into {100} silicon, (with a 15 Å SiO_2 layer, 0.5° divergency) comparison between SIMS profiles [4,48] and the current work simulation results.

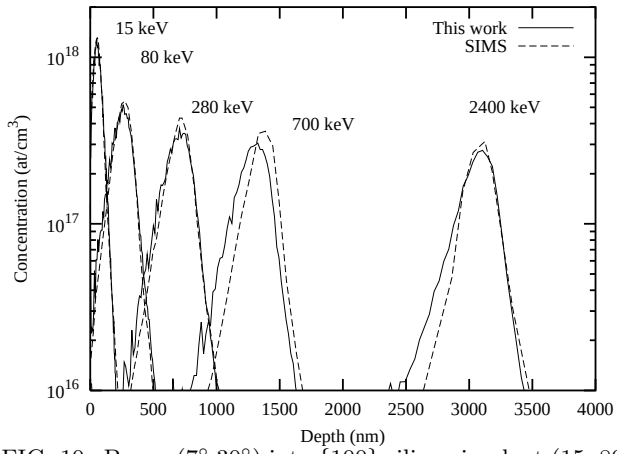

FIG. 10. Boron (7°,30°) into {100} silicon implant (15, 80, 280, 700 and 2400 keV, with a 15 Å SiO_2 layer) comparison between SIMS profiles [4,16] and the current work simulation results.

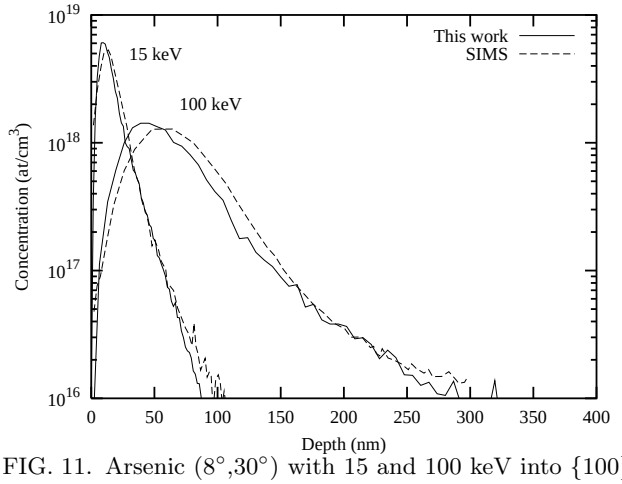

FIG. 11. Arsenic (8°,30°) with 15 and 100 keV into {100} silicon implant comparison between SIMS profiles [32] and the current work simulation results.

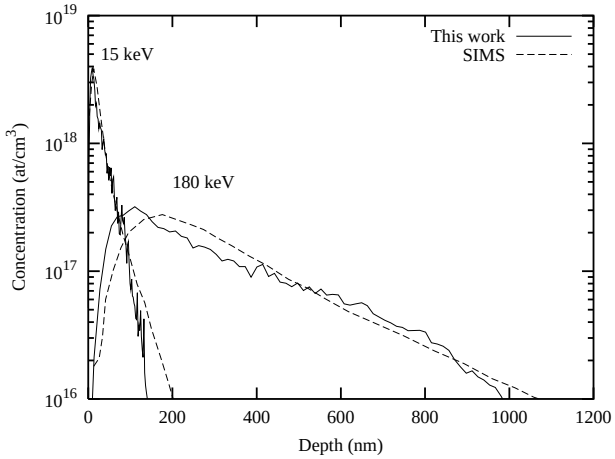

FIG. 12. Arsenic (0°,0°) with 15 and 180 keV into {100} silicon implant comparison between SIMS profiles [32] and the current work simulation results.

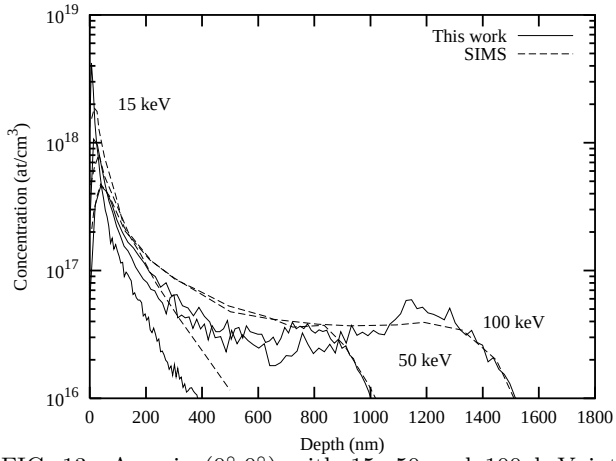

FIG. 13. Arsenic (0°,0°) with 15, 50 and 100 keV into {110} silicon implant comparison between SIMS profiles [16] and the current work simulation results.

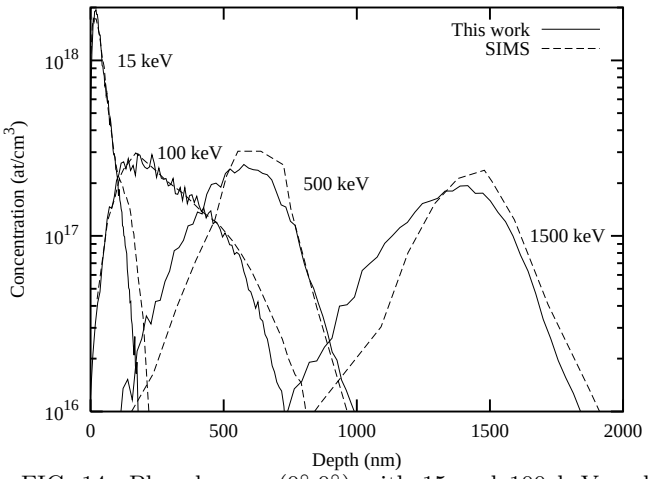

FIG. 14. Phosphorous (0°,0°) with 15 and 100 keV and phosphorous (10°,15°) with 500 and 1500 keV into {100} silicon implant comparison between SIMS profiles [21] and the current work simulation results.

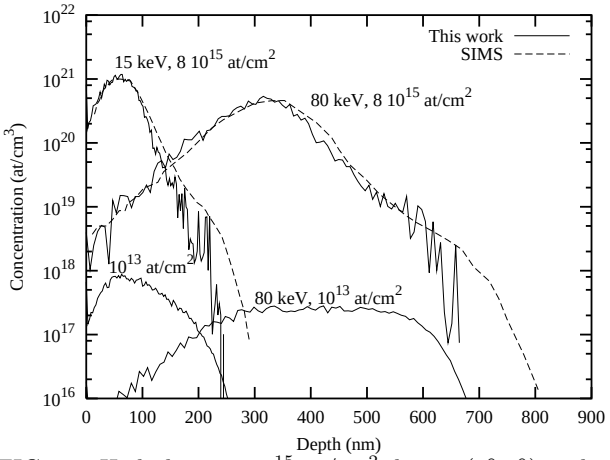

FIG. 15. High dose, $8 \cdot 10^{15}$ at/cm^2, boron (0°,0°) with 15 and 80 keV into {100} silicon implant comparison between SIMS profiles [16] and the current work simulation results. The low dose simulation results are also shown for comparison.

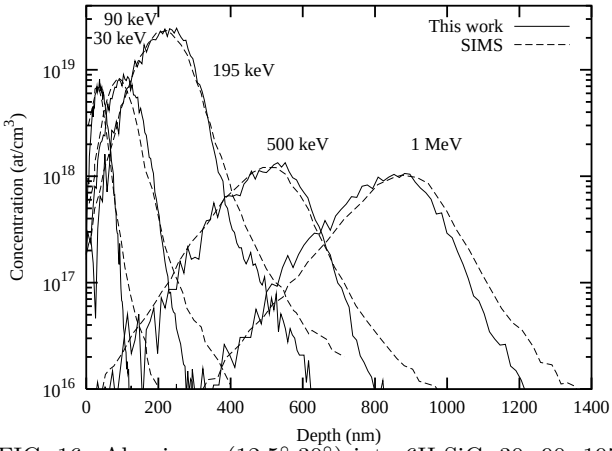

FIG. 16. Aluminum (12.5°,30°) into 6H-SiC, 30, 90, 195, 500 and 1000 keV implants with doses of $3 \cdot 10^{13}$,$7.9 \cdot 10^{13}$, $3.8 \cdot 10^{14}$, $3 \cdot 10^{13}$ and $3 \cdot 10^{13}$ at/cm^2 respectively. The orientation of the wafer flat is $\{11\bar{2}0\}$ and the wafers are cut 3.5° off-axis from the {0001} plane toward the $\{11\bar{2}0\}$ direction [46].

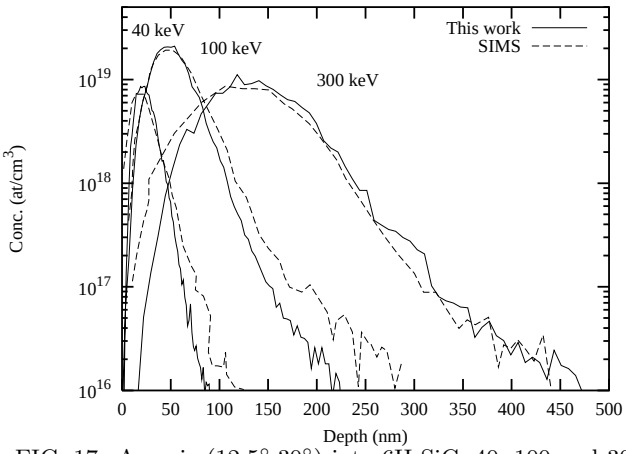

FIG. 17. Arsenic (12.5°,30°) into 6H-SiC, 40, 100 and 300 keV implants with doses of $2 \cdot 10^{13}$, $9.9 \cdot 10^{13}$ and $1.1 \cdot 10^{14}$ at/cm^2 respectively. The orientation of the wafer flat is $\{11\bar{2}0\}$ and the wafers are cut 3.5° off-axis from the {0001} plane toward the $\{11\bar{2}0\}$ direction [46].

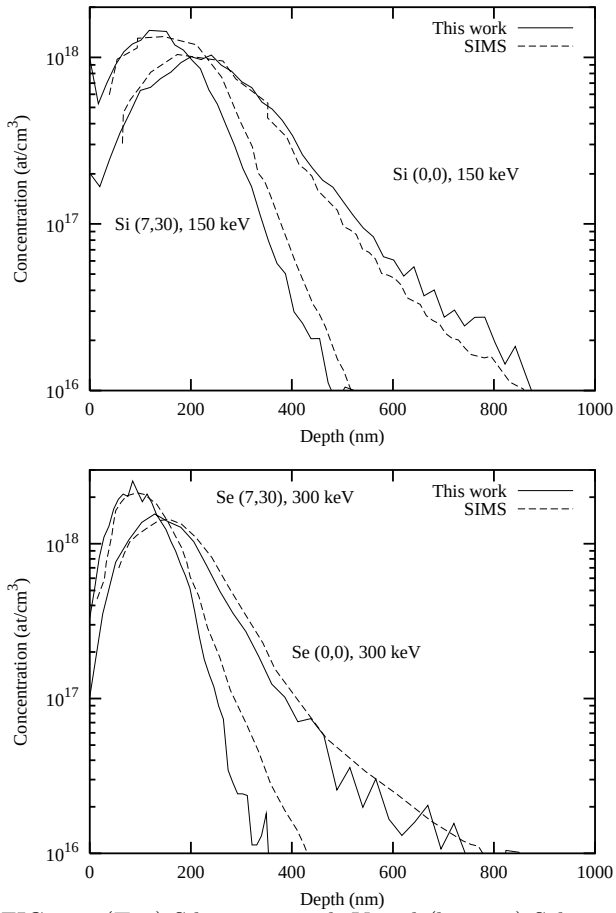

FIG. 18. (Top) Silicon at 150 keV and (bottom) Selenium at 300 keV (REO and {100} channel) implanted [47] into GaAs.